

## Microstructural behavior and mechanics of nano-modified cementitious materials

Nikolaos D. Archontas<sup>\*1a</sup> and S.J. Pantazopoulou<sup>2b</sup>

<sup>1</sup>Electrical & Computer Engineering Department, Democritus University of Thrace, 67100, Greece

<sup>2</sup>Department of Civil & Environmental Engineering, University of Cyprus, P.O. Box 20537, 1678 Cyprus

(Received August 27, 2014, Revised November 20, 2014, Accepted November 30, 2014)

**Abstract.** Ongoing efforts for improved fracture toughness of engineered cementitious materials address the inherent brittleness of the binding matrix at several different levels of the material's geometric scale through the addition of various types of reinforcing fibers. Crack control is required for crack widths that cover the entire range of the grain size spectrum of the material, and this dictates the requirement of hybrid mixes combining fibers of different size (nano, micro, macro). Use of Carbon Nano-Tubes (CNT) and Carbon Nano-Fibers (CNFs) as additives is meant to extend the crack-control function down to the nano-scale where cracking is believed to initiate. In this paper the implications of enhanced toughness thus attained at the material nanostructure are explored, with reference to the global smeared constitutive properties of the material, through consistent interpretation of the reported experimental evidence regarding the behavior of engineered cementitious products to direct and indirect tension.

**Keywords:** carbon nanotubes/nanofibers; constitutive relations; stress-strain; cementitious materials; fibers; bond; hybridization

---

### 1. Introduction

During the last decade the scientific community in structural concrete has been at the cross roads of ground-breaking developments that are motivated by the emergence of new technologies in the associated materials. Novel, high strength, durable reinforcements, and high performance cementitious materials hold promise for new innovative structural engineering forms and systems, greater strength-to-material ratios that will render possible much taller, safer, better performing structures. The leap from the advent in the array of development of available individual materials to the structural integration depends on the fracture toughness of the host cementitious matrix, as key to securing composite action between concrete and any form of innovative reinforcement; this action is essential whether the reinforcement comes in the form of bars, macro-fibers, or micro-fibers.

Composite action relies on mobilization of bond between the cementitious matrix and the composite reinforcement for stress-transfer. Being a state of shear stress at the reinforcing interface,

---

\*Corresponding author, Ph.D. (electronics), Research Physicist, E-mail: [narcho@ee.duth.gr](mailto:narcho@ee.duth.gr)

<sup>a</sup>Professor, E-mail: [pantaz@ucy.ac.cy](mailto:pantaz@ucy.ac.cy)

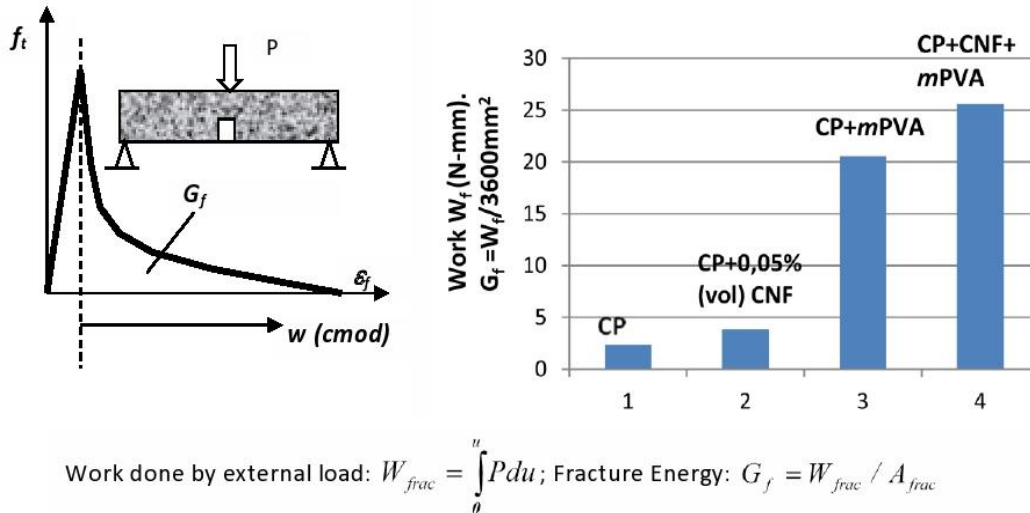


Fig. 1 Fracture energy in cementitious materials. (a) Definition from modulus of rupture tests, (b) Fracture work  $W_f$  obtained from 3-point load tests on  $63 \times 63 \times 250$  mm prisms in cementitious paste (CP) reinforced with hybrid fiber mixes (Konsta *et al.* 2011).

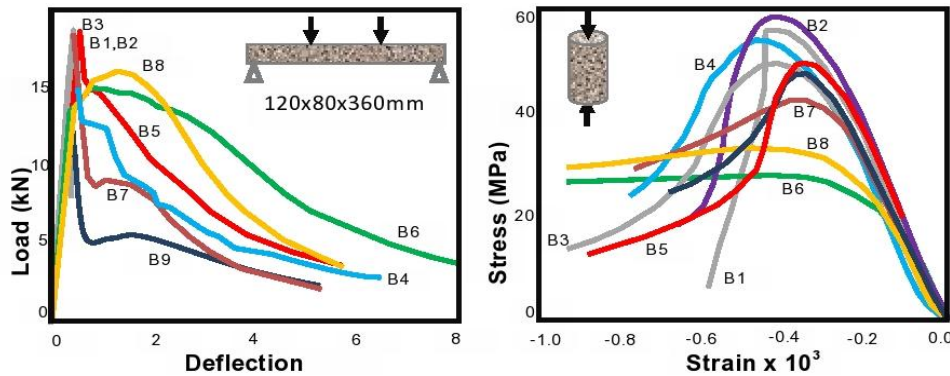


Fig. 2 Results from tests on hybrid mixes. (a) Modulus of rupture tests in micro-concrete with fiber mixes (b) Indirect characterization of fracture through uniaxial compression tests of the hybrid mixes studied in (a). (Nomenclature:  $mf$  = Steel Microfiber,  $sf$  = Steel Fiber,  $pf$  = Polypropylene Fiber. B1: 0% fiber, B2: 1% $mf$ , B3: 2% $mf$ , B4: 0.4% $mf$ +0.6% $sf$ , B5: 0.8% $mf$ +1.2% $sf$ , B6: 4% $pf$ , B7: 1.0% $mf$  + 1.5% $pf$ , B8: 2% $mf$  + 3% $pf$ , B9: 1.5% $pf$ .)

bond may be interpreted as diagonal tension in the bulk material surrounding the discrete reinforcing elements. This is because principal axes are inclined with respect to the shear stress, and one of the principal stresses is necessarily tensile, causing failure through tensile fracture in the absence of transverse confinement. Previous research has shown that unless the fracture toughness characteristic of the matrix is enhanced by several orders of magnitude, ultra high strength reinforcing products such as FRP (Fiber-Reinforced Polymer) bars and stainless-steel reinforcements which are available novel construction materials, cannot be fully integrated in conventional structural concrete. The reason is that these reinforcing bars possess much higher strengths than what can be supported in conventional concretes through the available bond -

tension mechanisms. So, even when used as high strength reinforcement, they can never develop their full strengths in the absence of significant external confinement unless the cementitious matrix possesses a high amount of fracture energy (Tastani and Pantazopoulou 2006).

Fracture energy, ( $G_f$ ), is a property that characterizes the cementitious material response in tension. It is associated with the post-peak softening branch that follows rupture (Fig. 1). For the needs of novel reinforcing products it is particularly important that an increase of toughness rather than of peak stress is desirable; that is, the ability of the material to sustain its strength for a large range of strain, even by slowing down or mitigating the rate of strength loss in the post-peak softening branch of the tensile stress-strain envelope.

Figs. 1(b) and 2(a) plot results from published modulus-of-rupture tests conducted on prismatic (beam) specimens with a variety of concentration of fiber reinforcing materials. It is evident from the experimental trends that hybrid mixes are more promising in supporting a sustained tensile resistance with increasing tensile deformation than what is seen in mixes containing a single fiber-type network. Note that the data plotted in Fig. 1(b) concern mixes of CNF (Carbon Nano-Fibers) and mPVA (i.e., micro Poly-Vinyl Alcohol fibers).

Evidence of improved performance in tension by the addition of fibers may also be traced in uniaxial compression tests: here, tensile strain occurs in the transverse direction, due to Poisson's effect, since failure of cementitious materials in compression is perpetrated by tension cracks running parallel to the compression field. Thus, in unreinforced cementitious matrices the phenomenological Poisson's ratio attains a value of 0.5 at peak compressive stress, and it increases further, to values exceeding  $\nu_{cr}=1$  near failure. Note that this expansive behaviour which is characteristic of the class of concrete materials, is controlled and mitigated by the addition of fibers, with consequent apparent ductility being evident in the post-peak descending branch in compression.

Although all the emphasis in characterizing CNT-reinforced mixes has been based on indirect tension tests (such as flexural testing of beams under three or four point loading), the relationship between ductility gain in compression and increased fracture energy effected by the addition of fibers has already been documented in other hybrid mixes such as those depicted in Fig. 2 (Pantazopoulou and Zanganeh 2001); furthermore, it has been shown through analytical studies that the same behavior is also expected in the case of CNT reinforcement (Balopoulos *et al.* (2014)). Examples of such findings are shown in Fig. 2 obtained from a variety of paired tests (i.e. four point bending on prisms  $120 \times 80 \times 360$  mm shown in Fig. 2(a) and cylinders in uniaxial compression in Fig. 2(b)) conducted on various microconcrete mixes. These mixes contained different volumetric ratios of fibers - the % number in the identification code represents volumetric ratios in the mix of the corresponding fiber type (see nomenclature in Fig. 2). This result underlines the favourable effect of hybridization, but most importantly, it highlights the significance of compression testing as an indirect means of assessment of the materials' response in tension.

## 2. Microstructural mechanics of cementitious materials and the role of CNTs/CNFs

At the root of the familiar tensile stress-strain response of conventional cementitious materials depicted in Fig. 3 lies the weak cohesive mechanism that holds the cement hydrate molecules together (owing to the amorphous state of this class of materials). At the nanoscale the phenomenon occurs due to the fast decay of intermolecular attraction (van-der Waals forces) with increasing separation distance as depicted in the Gordon-Morse diagram shown in Fig. 3(a). The implications of this characteristic are propagated and manifested at the micro, meso and macro

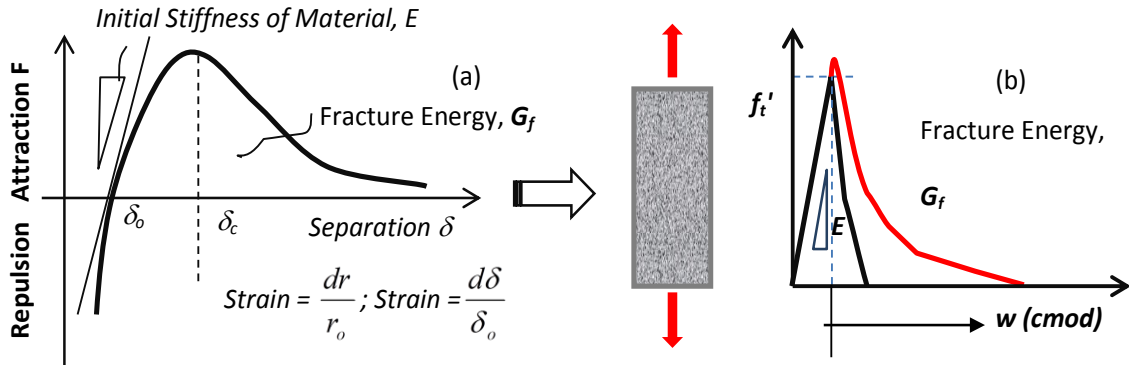


Fig. 3 The implications of the Gordon-Morse diagram on the macroscopic scale. (a) Intermolecular attraction/repulsion vs. separation distance, and definition of the notion of stress and strain in an average sense. (b) Typical response of brittle material in tension (from modulus of rupture tests): stress vs. crack-mouth opening displacement,  $w$  (cmod). Red line: Enhancement in fracture energy achieved by only a single type of fiber.

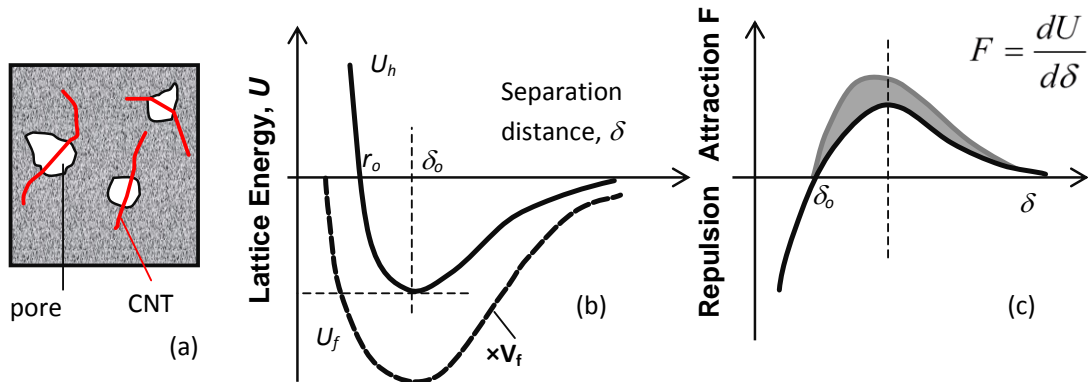


Fig. 4 Interlocking of CNTs in the gel: although at the nanoscale, it is a mechanical means to bridge molecule separation, supplementing the diminishing van-der Waals attraction. (a) Elementary volume of the reinforced hydrate, (b) Idealized Gordon-Morse Diagram of constituent materials (solid line:  $U_h$ =hydrate; dashed line:  $U_f$ =CNT contribution), (c) Corresponding effect in terms of effective attraction/repulsion (grey line in (c) is the resulting composite action).

material geometric scales by a persistently brittle response in uniaxial tension (Fig. 3(b)). Note that the enhancement in fracture energy achieved is always limited by the bond strength and development capacity of the type of reinforcement used (e.g. fibers of various sizes including CNTs).

Here the physical significance of the apparent modulus of elasticity of the material in Fig. 3(a) and 3(b) is also relevant. Thus, in Fig. 3(a),  $E$  is the rate of change of intermolecular attraction at

the equilibrium separation distance,  $\delta_o$ . In cementitious hydrates, where the hydration products are packed at a mean distance equal to the mean pore size, and pores are approximated as rectangular slits between gel macromolecule sheets, it has been demonstrated that  $\delta_o$  is about double the hydraulic mean radius,  $r_o$  (Pantazopoulou and Mills 1991). The hydraulic mean radius,  $r_o$ , is defined by the total pore volume,  $w_e$ , divided by their internal surface area, both being measurable and characteristic properties of the hydrate, i.e.,  $r_o = w_e / \Sigma_{BET}$ .

Here, the pore volume is taken equal to the evaporable water content of the cement hydrate,  $w_e$ , defined as the pore water lost on heating to 110° C.  $\Sigma_{BET}$  is the internal surface area of the pores, estimated as:  $\Sigma_{BET} = 3570V_m m^2/g$  of unhydrous cement;  $V_m$  is the monolayer capacity of water of the hydrated gel, assuming that the mean diameter of a water molecule = 10.6Å°;  $V_m$  is estimated from the chemically bound water  $w_n$ . All these parameters are linked to the water-cement ratio (Pantazopoulou and Mills, 1995), so that the following expression may be derived for the hydraulic mean radius:

$$r_o = \frac{w_e}{\Sigma_{BET}} = \frac{14.673w_oV_m \times 10^{-6}}{3570V_m} = 4.11 \times 10^{-9} w_o \text{ (in m)} = 4.11 \cdot w_o \text{ (in nm)} \quad (1)$$

For example, given a water-cement ratio,  $w_o=0.45$ , it follows that the mean pore radius in the gel is  $r_o=1.85 \times 10^{-9} m = 1.85 nm$  and the corresponding separation distance,  $\delta_o \div 3.7 nm$ . Thus, based on Fig. 3(a) and the definition of the hydraulic mean radius through its relation to the equilibrium separation distance, a direct link between the density of packing in the cementitious matrix and mechanical strength is possible. By definition, infinitesimal strain which is a measure of deformation in the material microstructure, actually represents the rate of change of the hydraulic mean radius (Fig. 3(a)) and of the interparticle distance in the direction considered (Pantazopoulou and Mills 1995) – the two alternative expressions of strain placed one against the other enable the user to relate the common notion of strain, which is a normalized length change as defined in the framework of homogeneous solids, to the size of the pores (and change thereof) which is specific to cementitious matrices. This is also used to establish a physico-chemo-mechanical framework for interpretation of the behaviour of cementitious materials under stress.

## 2.1 The effect of CNTs & CNFs

If the cementitious solid is weakly bound, then the attraction force decays beyond the critical separation distance,  $\delta_c$ , which is about  $2\delta_o$ . The force-separation regime may be approximated by simple functions of  $\delta$  such as the following:

$$f_t(\delta) = E \cdot \frac{(\delta - \delta_o)}{a(\delta - \delta_o)^2 + b} \quad (2a)$$

with  $a$  and  $b$  being determined from the requirement that peak force is developed at  $\delta_c = 2\delta_o$ , so that  $f_{t,max} = f_t(\delta = 2\delta_o)$  and  $f'_t(\delta = 2\delta_o) = 0$ , whereas  $f'_t(\delta = \delta_o) = E$ , so that  $a = 1/\delta_o^2$  and  $b=1$ , and  $E = 2f_{t,max}/\delta_o$ . This simplifies the above expression to,

$$f_t(\delta) = E \cdot \frac{(\delta - \delta_o)}{\frac{(\delta - \delta_o)^2}{\delta_o^2} + 1}; \text{ for } \delta = 10\delta_o \Rightarrow f_t(10\delta_o) = E \cdot \frac{9\delta_o}{81 + 1} = 0.22 f_{t,max} \quad (2b)$$

A more rapid degradation of force may be approximated by a symmetric curve just like the Hognestad parabola conventionally used to represent the stress envelope for cementitious materials, according to which the attraction force diminishes over a separation distance about twice the critical value – hence, macroscopically, the strain of the bulk material at total loss of load is about twice the magnitude attained at peak resistance:

$$f_t(\delta) = f_{t,max} \left( 2 \cdot \frac{\delta - \delta_o}{\delta_c - \delta_o} - \left( \frac{\delta - \delta_o}{\delta_c - \delta_o} \right)^2 \right) \xrightarrow{\text{for } \delta_c = 2\delta_o} f_t(\delta) = f_{t,max} \left( 2 \cdot \frac{\delta - \delta_o}{\delta_o} - \left( \frac{\delta - \delta_o}{\delta_o} \right)^2 \right) \quad (2c)$$

The area under the curve for  $\delta > \delta_c = 2\delta_o$  defines the associated fracture energy,  $G_f$ , of the material. Given the value of  $G_f$ , the above models enable estimation of the corresponding cohesive fracture strength, according with,

(a) From Eq. (2b):

$$f_{t,max} = \sqrt{\frac{G_f \cdot E}{2 \cdot \ln \left[ \frac{(\delta - \delta_o)^2}{2\delta_o^2} + \frac{1}{2} \right]}}, \text{ and, } G_f = f_{t,max} \cdot \delta_o \ln \left[ \frac{(\delta - \delta_o)^2}{2\delta_o^2} + \frac{1}{2} \right] \quad (2d)$$

(b) From Eq. (2c):

$$f_{t,max} = \sqrt{\frac{3 \cdot G_f \cdot E}{4}} \quad \text{and} \quad G_f = 2f_{t,max} \cdot \delta_o / 3 \quad (2e)$$

where,  $G_f$  in [N/m] is measured as the energy absorbed to create a unit fracture surface (i.e., a tensile crack of unit area). Note that for ordinary cementitious pastes,  $G_f$  varies from 22 to 26 N/m (Padevet and Zobal (2010)), and increases to 130 N/m for ordinary strength mortars and concretes (for an assumed compressive strength of 25MPa,  $G_f = 73(f_{cm}/10)^{0.18}$  N/m = 86 N/m, fib Model Code 2010). The two expressions converge when  $\delta - \delta_o = 2\delta_o$  (i.e., when the separation distance increases more than 3 times the value at the unstressed state).

In this framework, it is of interest to determine the function of additives such as CNTs and CNFs in enhancing the breadth and height of the fundamental curve in Fig. 3(a). According to the preceding, the microstructure of hardened binder which comprises a continuous matrix of Calcium-Silicate-Hydrate (C-S-H) has a porous structure that is a function of the equilibrium separation distance  $\delta_o$  in Fig. 3(a), with various products of hydration embedded). It is generally believed that cracks perpetrated at the macroscale of a densely packed cementitious composite would have to begin with some degree of separation between gel molecules. In this regard, CNT and CNF addition is motivated by the intent to control cracking at the nanoscale where this process

is believed to initiate. In the early attempts of mixing nano-reinforcement to cementitious matrices this benefit was overwhelmed by flaws due to bundling of CNTs that were often held responsible for causing premature crack initiation. However, with the use of pertinent technologies (e.g. sonication, Konsta-Gdoutos *et al.* (2010)), successful mixing has become possible so that the theoretical intent of reinforcing cementitious materials with CNTs may become feasible, as shown for example in Fig. 1(b) (cases 2 and 4).

SEM (Scanning Electron Microscope) images from Li *et al.* (2005) indicate that the primary function of CNTs crossing the amorphous domain that the heterogeneous hydration products provide, is mainly to bridge pores and starting cracks through interlocking action. Although additional functions have been associated with CNTs in cementitious matrices, such as an effective reduction of porosity (i.e., an apparent reduction in the hydraulic mean radius  $r_o$ , in Fig. 3(a) due to better packing of fine aggregates) and the development of covalent bonds between the calcium silicate hydrates and the CNTs when the latter have been previously treated with ionic plasma, crack bridging is the only function that may be relied upon for enhancement of macroscopic strength. The origin of increased packing density cannot be traced consistently throughout the tests (see for example results by Sakulich and Li (2011), whereas localized strengthening of interfacial bonding between C-S-H and the CNT's, which was obtained through treatment of the CNT, simply translates the plane of weakness further out to the next unstrengthened interface in the heterogeneous material; a consequence of this mitigation of the fracture plane further beyond the CNT – hydrate interface is not easily reflected in the macroscopic material response due to the natural tendency of the cracking plane to propagate through paths that completely bypass the stronger interfaces. It is in light of this fact that hybridization of reinforcing additives should be considered for improvement even in the case of CNT additions – (e.g., case 4 in Fig. 1(b)).

### 3. Modelling the function of the CNTs in the host amorphous matrix

CNTs mixed in cementitious matrices maintain the shape they had assumed when stirred in bulk in the fresh matrix; strings may be curled and wavy particularly in cases of longer lengths (Fig. 4(a)). For this reason, in modelling their interaction with the hardened matrix in this work, their contribution is only considered when resisting interparticle separation, whereas they are considered inert in the case of contraction (interparticle repulsion; see Fig. 4(b) and 4(c) which illustrates the interlocking action of CNT's in the gel). Here the lattice energy  $U$  of the composite is postulated to comprise contributions of the respective lattice energies of the hydrate and of the CNTs fixed in the solid structure of the matrix, respectively. In this context, the lattice energy of the CNTs is scaled to the volume fraction of the additive,  $V_f$ , (e.g., volumetric ratio of fibers):

$$U = U_h + V_f \times U_f \quad (3a)$$

where,  $U_f$  is non-zero only in the lower part of the diagram. A commensurate effect is noted in the average interparticle force diagram (Fig. 4(c)), which is derived upon differentiation of the lattice energies ( $F = dU/d\delta$ ); the grey area represents the average strength increase imparted by the various mechanisms of interaction between CNTs and cementitious paste at the nanoscale level.

Note that a relatively simple model for  $U_h$  that is compatible with the force attenuation relationship given in Eq. (2c) has the form:

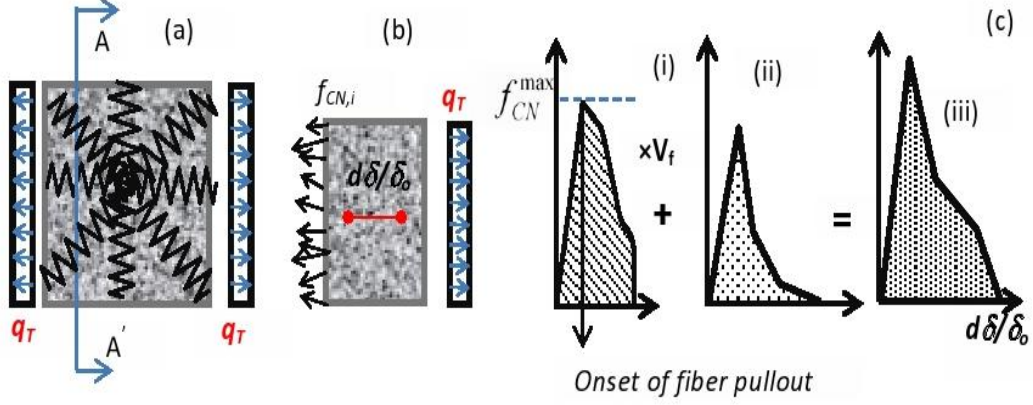


Fig. 5 (a) Mechanistic Model of the CNT restraining function. (b) Function of CNT as active reinforcement under a tension stress field,  $q_T$ , causing collinear tensile strain  $d\delta/\delta_o$  normal to the cross section A-A'. (c) Strain energy density contributions: (i) stored in CNTs; apparent yielding corresponds to the onset of fiber pullout, (ii) stored in the cementitious matrix, (iii) total fracture energy.

$$U_h(\delta) = \int f_i(\delta) d\delta = \frac{E\delta_o^2}{2} \cdot \ln \left| \frac{(\delta - \delta_o)^2}{\delta_o^2} + 1 \right| + C \quad (3b)$$

With the constant of integration  $C$ , obtained from the requirement that  $U_h(\delta = r_o = \delta_o / 2)$ , it follows that

$$U_h(\delta) = \frac{E \cdot \delta_o^2}{2} \cdot \ln \frac{4}{5} \cdot \left[ \frac{(\delta - \delta_o)^2}{\delta_o^2} + 1 \right] \quad (3c)$$

Provided that sufficient dispersion is obtained through the mixing process, an idealized model of the function of the CNTs in an elementary volume of the cementitious matrix is depicted in Fig. 5; springs are unidirectional, isotropically distributed in random orientations whereby the angle of inclination with respect to any axis of reference is assumed to follow a normal (Gauss) distribution (Fig. 5(a)). With this approach, any type of mass reinforcement such as CNFs or CNTs effects kinematic restraint against particle separation, in a manner analogous to conventional reinforcement in the macroscopic scale (Fig. 5(b)). In this context, the role of the reinforcing material is evaluated through the effected increase in fracture toughness ( $\Delta G_f$  value) and by the plastic separation distance (maximum distance beyond  $\delta_c$  over which the effective particle attraction remains undiminished); the model is expressed mathematically through the mechanical properties of the CNTs/CNFs, the volumetric fraction of fibers and the intrinsic properties of the mortar host matrix.

### 3.1 The effect of fiber distribution and orientation

The randomness of fiber distribution imparted by adequate mixing energy can only be modeled by a normal curve as, in the absence of specific measures to impart specific fiber orientation, the mixing process generates a uniformly random orientation. Deviations from this generic model could be justified, either in cases of clotting and agglomeration, or, in the case of short nanofibers, near the surface of large cement grains due to hydration from the outside inwards) (Tyson *et al.*, 2011). Note here that a normal distribution for fiber orientation corresponds to thoroughly smeared fibers, but this assumption would be totally irrelevant for test results obtained with poorly mixed CNTs / CNFs. Such mixes could fail to produce any positive mechanical influence by the additives and could, instead, compromise material strengths.

To quantify the effectiveness of the network of CNT strings as distributed reinforcing elements, considering that any given string is generally not perpendicular to the arbitrary section considered, an effectiveness coefficient,  $\lambda_{eff}$  is introduced. For truly random distribution of the fiber reinforcing network, a Gaussian distribution for the fiber/tube orientation-angle,  $\theta_f$  is assumed. Note that  $\theta_f$  is measured between the string axis and the plane of intersection, and ranges from 0 to 180 degrees. Therefore,  $\lambda_{eff}$  is calculated from,

$$\lambda_{eff} = \int_0^{\pi} \sin \theta_f d\theta_f \quad (4)$$

It can be shown that  $\lambda_{eff}=0.5$  which implies that in a truly random distribution, only 50% of the fibers are effective in normal tension at any arbitrary cross section through the material mass. A question of practical value is to determine the number of CN strings or fibers that are crossing a unit area of the composite,  $\bar{n}_{CN}$ . To estimate this variable, reference need to be made to an elementary volume  $v_o$ , having dimensions of the same length as that of the string in consideration,  $L_{CN}$ , i.e.,  $v_o = L_{CN}^3$ . From the volumetric ratio of the strings in the composite ( $V_f$ ) and from a single string volume, which is equal to:  $L_{CN} \cdot \pi \cdot d_{CN}^2 / 4$  (where  $d_{CN}$  the diameter of the string's cross section), the total number of CN strings (tubes or fibers) contained in  $v_o$  may be estimated:

$$N_{CN} = \frac{4 \cdot V_f \cdot L_{CN}^3}{\pi \cdot d_{CN}^2 \cdot L_{CN}} \approx 1.25 \cdot V_f \left( \frac{L_{CN}}{d_{CN}} \right)^2 \quad (5)$$

Ideally, if bundling of tubes/fibers is avoided, a random cross section in the elementary volume crosses half the number of strings contained; therefore the number of tubes/fibers crossing an elementary area  $L_{CN} \times L_{CN}$  of the composite is approximated as,  $n_{CN}=0.5N_{CN}$ , and for a unit area,

$$\bar{n}_{CN} \approx 0.625 \cdot V_f \left( \frac{L_{CN}}{d_{CN}} \right)^2 \quad (6)$$

### 3.2 Function of CNTs in tensile resistance (restraint to separation // to tension load)

In a state of pure tension as illustrated in Fig. 5(b), under the normal tensile stress  $q_T$ , the

applied load increases the interparticle distance, and therefore, attraction forces resist the tensile deformation (defined by the rate of change in separation distance,  $\varepsilon_t = d\delta/\delta_o$ ) up to a point  $\delta_c$  that corresponds to the limit in the restoring capacity of the particles (macroscopically this is the point where peak stress is attained). Fracture corresponds to strains that exceed the amount  $(\delta_c - \delta_o)/\delta_o$ . The  $i$ -th CNT string or fiber crossing the section plane, A-A', develops a stress  $f_{CN,i}$  in response to tensile deformation. The stress resultant of the tensile stress in the binder and of the CNT forces, normal to the section cut A-A' is:

$$f_{i,CNT} = f'_i + \lambda_{eff} \cdot \bar{n}_{CN} \cdot a_{CN} \cdot \bar{f}_{CN} = q_T \Rightarrow f'_i + \lambda_{eff} \cdot \frac{V_f}{2} \cdot \bar{f}_{CN} = q_T \quad (7a)$$

where,  $a_{CN}$  the cross-sectional area of a single tube/fiber ( $= \pi \cdot d_{CN}^2 / 4$ ) and the mean CNT stress is

$$\bar{f}_{CN} = k_{CN} \cdot \frac{d\delta}{\delta_o} \leq f_{CN}^{max} \quad (7b)$$

and  $\bar{n}_{CN}$  is the characteristic count of CNTs/CNFs per unit area at an arbitrary section of the hydrate defined by Eq. (6). The bar symbol on the tube/fiber stress represents the mean value over the  $\bar{n}_{CN}$  strings,  $\bar{f}_{CN}$  is the axial stress of the tube or fiber,  $k_{CN}$  is the average isotropic stiffness of the CNT/CNF system in the binder mass, and  $f_{CN}^{max}$  is the nominal development capacity of a CNT/CNF in the binder. As illustrated in Fig. 5(c)-(i) fiber axial stress is limited by its interfacial bond with the surrounding matrix, and as such, it is limited by pullout failure. The first term in Eq. (7a) represents the intrinsic tensile strength of the cementitious binder; this term is represented by the stress-strain diagram of graph (ii) in Fig. 5(b); it diminishes after tensile rupture of the binder due to its brittle response. Based on Eq. (7a) it follows that the tension strength increase observed in nano-reinforced cementitious mortars is proportional to the volume ratio of the fibers in the mix, and to the peak development capacity which depends on the properties of the tube/fiber interface with the cementitious binder.

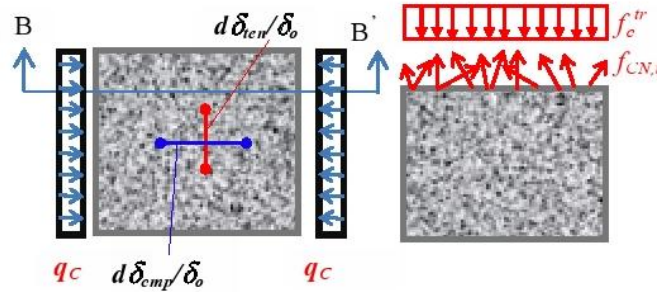


Fig. 6 Passive confinement function in directions orthogonal to the compression stress field  $q_c$ , under a transverse tension strain field  $d\delta/\delta_o$  owing to Poisson- effect. Estimation of equivalent lateral confining pressure,  $f_c^{tr}$  in the bulk material. (Indices: cmp=compression, ten=tension)

The work done by the fibers in restraining the value  $\delta$  of up to any given level of strain  $d\delta/\delta_o$ , is stored in the lattice, in the form of strain energy over and above the corresponding intrinsic lattice energy of the basic host matrix as illustrated in Fig. 5(b). In assessing the fracture toughness from tests and with reference to Fig. 4(b), the effective strain energy enhancement is obtained from the difference in toughness between modified and basic material response, as shown below:

$$U_f \times V_f = \left[ \frac{1}{2} \int_V k_{CN} \cdot \left( \frac{d\delta}{\delta_o} \right)^2 dV \right] \times V_f \leq \left[ \frac{1}{2} \int_V f_{CN}^{max} \cdot \frac{d\delta}{\delta_o} dV \right] \times V_f \quad (8)$$

Therefore, in securing increased deformation capacity in the cementitious material, the bond-slip relationship of the tubes/fibers is critical: note that little resistance to pullout is reportedly seen when using CNTs as compared to CNFs, due to the flaky nature of the lateral surface of the latter which promotes better mechanical interlock with the matrix.

### 3.2 Confining role of CNTs (restraint to transverse expansion)

Similarly, in a state of pure uniaxial compression as illustrated in Fig. 6 under normal compression stress,  $q_c$ , a field of transverse tensile strain is developed owing to a Poisson-like phenomena (transverse expansion to enable equilibrium of interparticle forces after longitudinal contraction). Consideration of equilibrium of normal stresses across a section B-B' highlights mobilization of a passive confining pressure  $f_c^{tr}$  required in order to counteract the stress resultant of the CNT forces normal to the B-B' section. It is considered that failure in compression for all brittle or semi-brittle materials (such as the cementitious host matrix) is triggered or, rather, associated with loss of cohesion in the direction orthogonal to the load owing to excessive particle separation (macroscopically this corresponds to a tensile strain approximately half the corresponding imposed compressive strain). It is evident that  $f_c^{tr}$  effectively substitutes for cohesion, thereby delaying failure. The equivalent transverse confinement in this case is,

$$f_c^{tr} = -\lambda_{eff} \cdot \bar{n}_{CN} \cdot a_{CN} \cdot \bar{f}_{CN} \quad (9a)$$

$$\bar{f}_{CN} = E_{CN} \cdot \frac{d\delta}{\delta_o} \leq f_{CN}^{max} \Rightarrow \frac{d\delta}{\delta_o} \Big|_{max} = \frac{f_{c,max}^{tr}}{\lambda_{eff} \cdot \bar{n}_{CN} \cdot a_{CN} \cdot E_{CN}} \quad (9b)$$

Again, the peak CN fiber / tube development capacity,  $f_{CN}^{max}$  is limited entirely by either the tensile strength (for CNFs) or by the frictional strength (for CNTs due to their smooth surface) of the calcium hydrates that form the basis of the hardened solid. Because this strength is rather low, it is evident that the ultra-high strength of the CNF/CNT additives cannot be realized in practice; yet, additives with a higher specific surface area have optimized interfacial conditions, and therefore they can effect a more dependable range of sustained plastic separation.

Lateral restraint in compression is reflected in the material stiffness by delaying or mitigating damage due to transverse expansion normal to the direction of principal compression, leading to a commensurate increase in compressive stress,  $\sigma_c$ , which is mobilized in response to an applied coaxial strain  $\varepsilon_c = \delta \cdot \delta_o / \delta_o = d\delta / \delta_o$ :

$$\sigma_c = E_d \cdot \varepsilon_c = E_d \cdot \frac{d\delta_{cmp}}{\delta_o} \quad (10a)$$

$$E_d = E \cdot \frac{1}{1 - 2 \frac{d\delta_{ten}}{\delta_o} \left/ \frac{\delta_c - \delta_o}{\delta_o} \right.} \leq E \quad \text{for } \bar{f}_{CN} \leq f_{CN}^{max} \quad (10b)$$

For  $\delta > \delta_c$ , the above reverts to the damaged  $E$  modulus of the conventional matrix material (see Pantazopoulou and Mills 1995).

The analytical expressions of the model detailed in the preceding sections are corroborated against the available experimental evidence in the following section. To this end, all reported data found in the literature were assembled into a single database for collective evaluation of the results. In many aspects the available data is rather limited and particularly varied due to the many alternative nano-materials that have been added for reinforcement

#### 4. Relevance with test results

The available experimental evidence regarding the mechanical properties of nano-reinforced cementitious matrices is summarized in Tables 1 and 2; data are organized separately for mortars and pastes and are grouped according with the study of origin (the numeral in the left column is the ID number of the experimental study included in the database; the corresponding reference is listed in Table 3). Note that tests are remarkably limited particularly when considering the

Table 1 Available tests on cementitious mortars, reinforced with MWCNTs

Ref. #	Sample	CNT type	CNT/C (%)	$f_c$ (MPa)	$f_t$ (MPa)	FE (N/m)
4	W/C=0.35	Plain		62		70
		L=3 $\mu$ m	0%~ 0,038 in	3.5%: 59		69
		D=30nm	initial mixing	7%: 51-65		69
			w/ Cement.	14%: 49		71
				30%: 42		74
5	Prisms 40x40x160	Plain			7.73	
L=700 $\mu$ m		0.5%		10.8		
6	W/C=0.45 0.45/1/1.5	Plain		52.27	6.69	
		L=12 $\mu$ m	0.5%	47.51	8.14	
		D= 6mm				
40x40x160	0.45/1/1.5	L=250 $\mu$ m	0.5%	62.13	8.37	
		D=20nm				
9	W/C=0.5 0.5/1/3	Plain		47.2		
			0.5%	51		
		D <100nm	1%	51.8		

$\Delta_u$  = Peak Displacement at Failure (mm);  $FE$  = Fracture energy per unit area of fracture (N/m);  $f_t$  = Flexural Strength, (MPa);  $E_o$  = Modulus of elasticity (GPa);  $\varepsilon_u$  = Ultimate Strain %;  $Tgh$ =Modulus of Toughness

Table 2 Available tests on cementitious pastes, reinforced with MWCNTs

Ref #	Sample	CNT type	CNT %C (by weight)	$f_c$ (MPa)	$f_t$ (MPa)	$FE$ (N/m)	$A_u$ (mm)	$E_o$ (GPa)	$\epsilon_u$ %	$T_{gh}$
1	MWCNT W/C=0.4 Prisms: 40×40×160	Plain		65	7.5					
		L=300 $\mu$ m D=60 nm	0.5%	71.87	10.1					
		L=700 $\mu$ m D=60 nm	0.5%	76.25	8.3					
		L=50 $\mu$ m D=15 nm	0.5%	9.37	2.9					
2	MWCNT W/C=0.4 Prisms: 65×65×160	Plain			3.25			14.4	0.041	0.6 <sup>(i)</sup>
		L=20 $\mu$ m D=8 nm	0.04%		4.9			15.3	0.032	0.9 <sup>(i)</sup>
			0.1%		5.25			13	0.042	0.8 <sup>(i)</sup>
		L=1.5 $\mu$ m D=9.5nm	0.04%		3.8			12.4	0.052	1.0 <sup>(i)</sup>
			0.1%		4.4			15.2	0.065	1.8 <sup>(i)</sup>
		0.2%		11.9			17	0.063	3.7 <sup>(i)</sup>	
3	MWCNT W/C=0.4 Prisms 65×65×160. Mixes as in group 10 [2]	Plain			8.8		0.35	15.2		0.22 <sup>(ii)</sup>
		L=1.5 $\mu$ m D=9.5 nm	0.1% UT		4.5		0.35	16.2		0.17 <sup>(ii)</sup>
			0.2% UT		12.0		0.42	18.8		0.38 <sup>(ii)</sup>
		L=65 $\mu$ m D=105 nm	0.1% UF		14.1		0.60	15.4		0.62 <sup>(ii)</sup>
		0.2% UF		12.7		0.37	24		0.30 <sup>(ii)</sup>	
4	W/C=0.35 initial mixing of fibers with Cement.	Plain		56		16.6				
			0.035%	70		18				
		L=3 $\mu$ m D=30 nm	0.07%	65		17.5				
			0.14%	52		19.8				
		0.3%	55		18.8					
7	W/C=0.5 SDS: (treated CNTs)	Plain		84	3.0					
		L=20 $\mu$ m D=10 nm	0.05%	51	2.7	(3.6)				
			0.25%	(58)	(3.6)					
8	W/C=0.5 Brij35: (treated CNTs)	L=200 $\mu$ m D=30 nm	0.05%	86	3.1					
			0.25%	71	3.2	(58)				
		Plain		84	3.0					
		L=20 $\mu$ m D=10 nm	0.05%	85	4.5					
			0.25%	81	4.1	(79)	(4)			
8	Brij35 W/C=0.5 Paste W/C=0.4	L=200 $\mu$ m D=30 nm	0.05%	92	3.4					
			0.25%	71	3.4	(79)	(4)			
		Plain		39.07	5.56					
				44.82	7.58	(48.4	(6.7)			
			0.5% (4)	9)						
	L=170 $\mu$ m D=80 nm	0.75%	37.92	6.9						
				27.58	5.86	(23.9	(4.37)			
		1% (4)		0)						



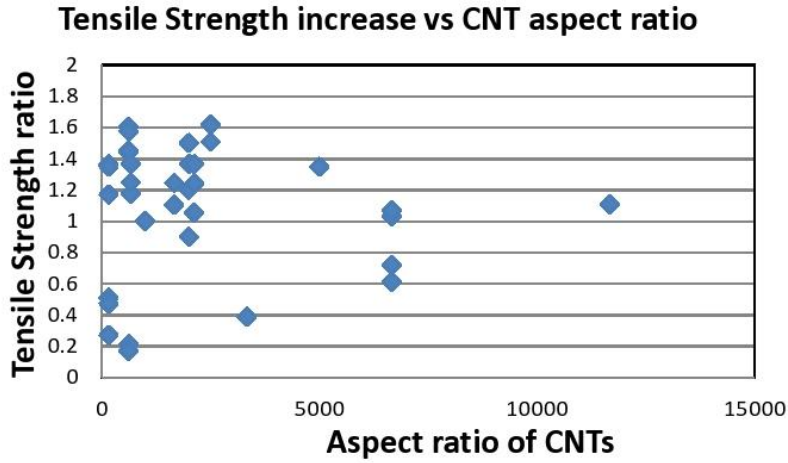


Fig. 7(a) Normalized tensile strength increase as a function of the aspect ratio

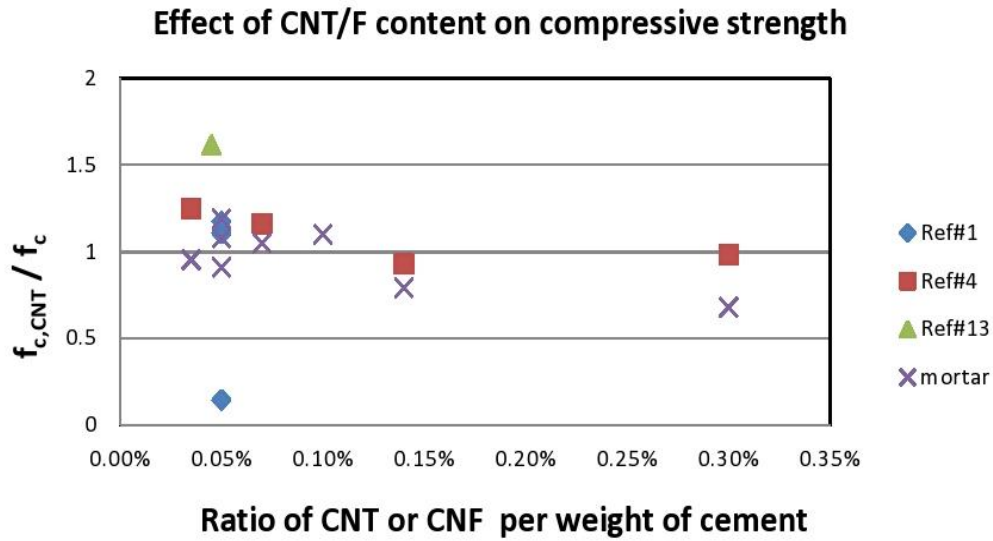


Fig. 7(b) Normalized compressive strength vs CNT content.

variability of parameters examined in the available databank and the small number of independent teams reporting (Table 3). (Functionalized hybrid mixes that combine other reinforcing additives except nanomaterials –such as other microfibers - are not included in the table since the objective is to identify from the available tests the benefit imparted by CNTs and CNFs). Listed in the table are, the CNT/CNF characteristics (length, diameter and content per weight of cement, measured tensile strength (usually from modulus of rupture tests with prism dimensions as listed), and measured compressive strength (where reported). In the published experimental studies, the content of added fibers,  $M_f$ , is given in terms of fiber weight per unit weight of cement; the weight

content of cement in the hydrate is denoted by  $c$ . To convert  $M_f$  to a volumetric ratio,  $V_f$  (i.e. the volume of fibers per unit volume of hydrate), the density of cement,  $g_c$ , and of the fibers,  $g_f$ , may be used as follows (usual values are,  $g_c=3.22 \text{ gr/cm}^3$ ,  $g_f=1.35 \text{ gr/cm}^3$ ):

$$V_f = \frac{M_f \cdot c \cdot \frac{1}{g_f}}{\left(\frac{c}{g_c} + w_o \cdot c\right)} = \frac{M_f}{\frac{1}{g_c} + w_o} \cdot \frac{1}{g_f} = \frac{M_f}{0.419 + 1.35w_o} \quad (11)$$

In the case of the database tests, most mixes were designed with  $w_o=0.4$ , and therefore,  $V_f \approx M_f$  in most cases.

Some tests report the measured Fracture Energy (in N/m, calculated from the area under the Load –displacement curve normalized by the specimen’s cross sectional area), whereas few others report the Modulus of Toughness (Tgh) values (in kPa, MPa, or  $\text{J/m}^3$ , calculated from the area under the tensile stress-strain curve); either of these variables is a measure of the toughness variability of parameters examined in the available databank and the small number of independent teams reporting (Table 3). (Functionalized hybrid mixes that combine other reinforcing additives except nanomaterials –such as other microfibers - are not included in the table since the objective is to identify from the available tests the benefit imparted by CNTs and CNFs). Listed in the table are, the CNT/CNF characteristics (length, diameter and content per weight of cement, measured tensile strength (usually from modulus of rupture tests with prism dimensions as listed), and measured compressive strength (where reported). In the published experimental studies, the content of added fibers,  $M_f$ , is given in terms of fiber weight per unit weight of cement; the weight

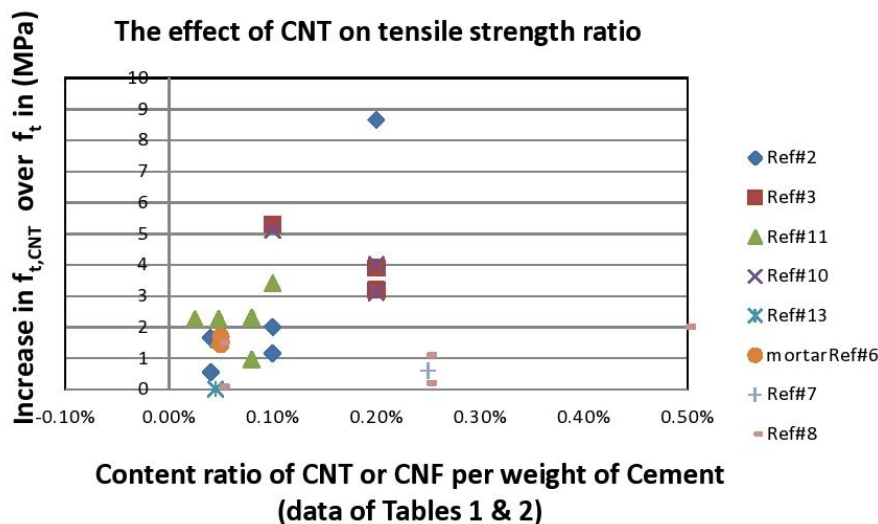


Fig. 8 Increase in cohesive strength by the addition of CNF/CNT, versus  $M_f$  of  $V_f$  (values obtained with reference to the corresponding properties of the plain mix)

content of cement in the hydrate is denoted by  $c$ . To convert  $M_f$  to a volumetric ratio,  $V_f$  (i.e. the volume of fibers per unit volume of hydrate), the density of cement,  $g_c$ , and of the fibers,  $g_f$ , may be used as follows (usual values are,  $g_c=3.22 \text{ gr/cm}^3$ ,  $g_f=1.35 \text{ gr/cm}^3$ ):

$$V_f = \frac{M_f \cdot c \cdot \frac{1}{g_f}}{\left(\frac{c}{g_c} + w_o \cdot c\right)} = \frac{M_f}{\frac{1}{g_c} + w_o} \cdot \frac{1}{g_f} = \frac{M_f}{0.419 + 1.35w_o} \quad (11)$$

In the case of the database tests, most mixes were designed with  $w_o=0.4$ , and therefore,  $V_f \approx M_f$  in most cases.

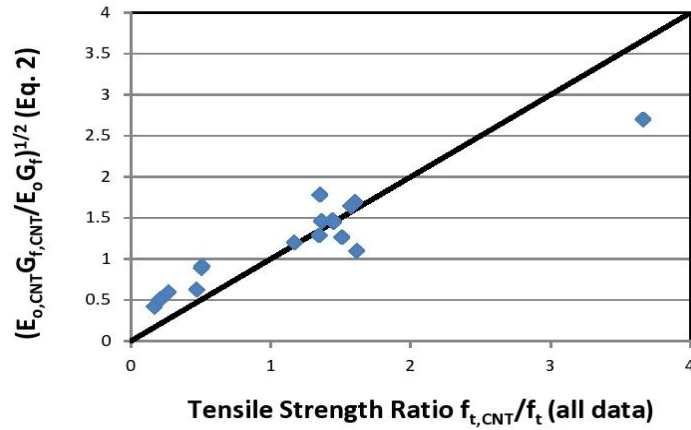


Fig. 9 Correlation of the test results with Eqs. 2(d) & (e)

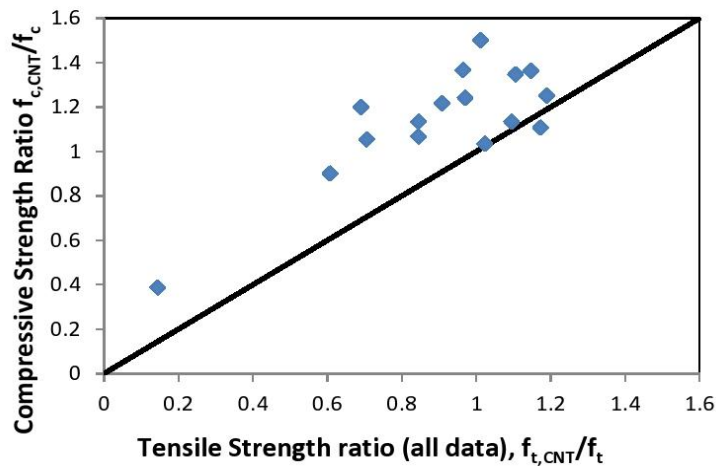


Fig. 10 Compressive versus tensile strength increase (values normalized with respect to corresponding properties of the plain mix)

Some tests report the measured Fracture Energy (in N/m, calculated from the area under the Load –displacement curve normalized by the specimen’s cross sectional area), whereas few others report the Modulus of Toughness (Tgh) values (in kPa, MPa, or J/m<sup>3</sup>, calculated from the area under the tensile stress-strain curve); either of these variables is a measure of the toughness enhancement effected by the nano-reinforcement provided. Plain refers to the basic mix;  $L$  and  $D$  are the mean length and diameter of CNTs / CNFs.

A remarkably wide variety of CNT and CNF additives have been considered in the available tests, the aspect ratio and length of fibers varying significantly between different studies. Fig. 7(a) plots the normalized tensile strength of the CNT-reinforced mix over that of the plan mix) against the CNT aspect ratio ( $L/D$ ). Most points lie in the range from 1-1.5 for the strength ratio, with an average strength increase in the range of 20% over the plain-mix value. Signs of poor dispersion are points lying below the value of 1 (i.e. with a strength ratio < 1). Similarly, Fig. 7(b) plots the compressive strength ratio against the weight ratio of the reinforcement (weight of CNTs per unit weight of cement); as seen in the tensile strength values, problems with mixing persist in this type of tests also as seen by the points between the  $y = 1$  line. Despite the scatter generated by the mixing difficulties, the data in Table 2 confirm that longer CNTs are more effective in improving the tensile and compressive strength of both pastes and mortars, underscoring the fact that the longer they are, the greater their effectiveness in arresting crack-growth that would otherwise tend to by-pass shorter CNT lengths (see for example data groups 5 and 6). Short CNTs are particularly ineffective in the case of mortars; a few of the cases where strength reduction is noted correspond to higher weight ratios of additives, apparently due to the hydrophobic nature of the CNTs. For the smaller amounts used there is an increasing tendency in strength measures with percent ratio of CNT/CNF additive (see Fig. 8, where the y-axis plots the increase in strength attained in excess of the reference plain value, expressed in MPa); aberrations to the rule do exist, owing to the difficulties in mixing these types of products in cement.

Due to the range of reported variables, the tensile strength increase owing to the addition on CNTs/CNFs may be correlated according with Eq. 2(d) and 2(e), with the square root of the ratios of moduli of elasticity times the energy ratios of nano-engineered composite to that of plain mix of identical composition (Fig. 9). In applying Eq. 2(d) to the data it is assumed that the mean separation distance  $\delta_0$  remains unaffected by the addition of the nano-reinforcements as postulated in (Fig. 4); the results plotted in Fig. 9 confirm this aspect of the proposed model. (Note that the same plot is produced for Eq. 2(e) when taking the ratio of  $f_{i,CNT}/f_t$ , where  $f_{i,CNT}$  is the peak cohesion of the CNT-reinforced matrix).

Tensile resistance is more effectively enhanced in the case of CNFs than CNTs according with the experiments, and consistently with Eq. 5 of the proposed model which relates the tensile strength of the composite with the pullout resistance of the reinforcement (CNFs have greater surface roughness than CNTs engaging a greater value for  $f_{CN}^{\max}$  according with Eq. 5(b) – see for example the data from groups 3 and 10. For the cases where available, data pairs of compressive and tensile strength values of the examined composites are plotted in Fig. 10. Values have been normalized with the corresponding properties of the respective plain mix. The linear trend implies that both strength parameters increase proportionately with the addition of CNTs / CNFs, confirming the premise of the model that the tensile strength of the reinforcements, which depends on the development capacity  $f_{CN}^{\max}$  of the tubes/fibers affects the mechanisms of resistance in the same manner both in tension and in compression as demonstrated in the preceding model from first principles (Eqs. 7-9). Note that with reference to the corresponding plain mixes,

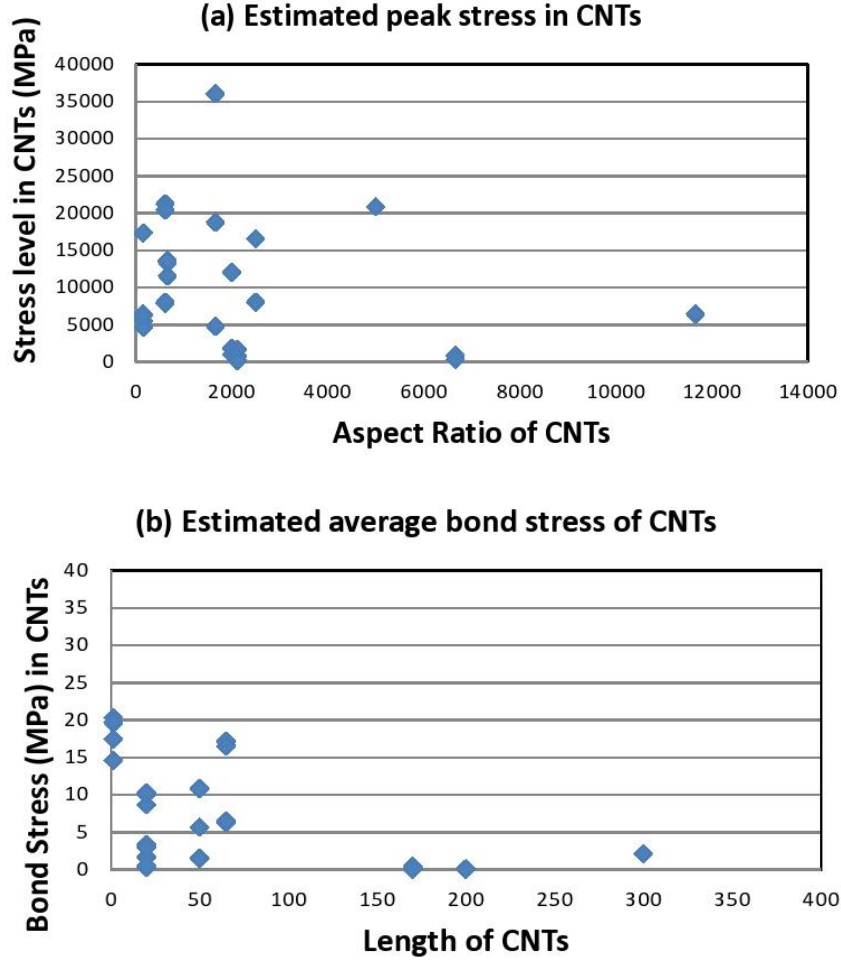


Fig. 11 (a) Peak developed stress in the CNT / CNF reinforcement as a function of the aspect ratio of the strings. (b) Average Bond Stress in the CNT/CNF reinforcement

whose properties are used for normalizing the strengths of the nano-composites, it is seen that the increase in tensile strength, compressive strength and fracture energy, ranges between 10% and 50% of the plain values.

Another point of interest is to establish the magnitude of axial stress that develops in the CNTs when the cementitious composite is stressed in tension: to find the peak average fiber stress, the increase in tensile strength of the composite (in MPa) is obtained (see Fig. 8). The value is set equal to the second term in Eq. 7(a) of the proposed model, as follows:

$$\Delta f_t' = f_{t,CNT}' - f_t' = \lambda_{eff} \cdot \bar{n}_{CN} \cdot a_{CN} \cdot \bar{f}_{CN} = \frac{V_f}{4} \cdot \bar{f}_{CN} \Rightarrow \bar{f}_{CN} = \frac{4 \cdot \Delta f_{ct}'}{V_f} \quad (12)$$

Using the mean stress estimate, the average bond stress,  $\tau$ , that develops on the lateral surface of the CNTs anchoring the resultant force per string is estimated, assuming that at most, half of the CNT length is available for anchorage (peak force development capacity). Therefore,

$$\tau = \frac{D_{CN}}{4} \cdot \frac{\bar{f}_{CN}}{L_{CN}/2} \quad (13)$$

Results obtained using Eqs. (12) and (13) in the tests of the database (where this calculation was possible given the scarcity of the data) are plotted in Fig. 11(a) and 11(b). Note that the stress levels attained in the CNT strings are significant, however the associated bond stresses are within the strength capacity range of common cementitious materials (below 20MPa). Also note that longer strings produce lower average bond stress consistent with the behavior of macroscopic reinforcement (where average bond stress for development of reinforcement strength is inversely proportional to the length of anchorage).

## 5. Conclusions

Ongoing efforts by the scientific community, aimed at improving the toughness of the cementitious materials address the inherent brittleness of the cementitious matrix at the nanolevel of the material geometric scale through addition of nano-fibers such as CNFs and CNTs. A fundamental objective in this process is to artificially increase and prolong the range of separation distance over which the intermolecular attraction may be considered as “*phenomenologically sustained*” through the mechanical interlock of fibers that bridge the separation gap. Most of the experimental results show that higher resistance to separation may be mobilized, but the corresponding range over which this resistance is sustained is affected to a lesser degree, so that the resulting fracture toughness increase is in the range of 15%. The same effects are observed in compression tests that indirectly account for the fracture toughness increase due to restrained expansion (pseudo-Poisson effect) normal to the compressive strain. Both effects are modelled through consistent interpretation of the notion of stress and strain in light of the fundamental principles of the physics of material microstructures. A database of the available tests is assembled providing a means by which to consistently evaluate the model’s fundamental assumptions and principles through the observed experimental trends. Poor dispersion due to the hydrophobic nature of the CNTs generally lowers the quality of the data obtained in many studies, however there is clear evidence of the enhancing contribution of this additive to both compressive and tensile strengths as well as fracture toughness. Further correlation of the model with additional experimental data when such become available would be needed in order to calibrate the various empirical coefficients (particularly the bond strength of the nano-reinforcements).

## Acknowledgments

This research has been co-financed by the European Union (European Social Fund – ESF) and

Greek national funds through the Operational Program "Education and Lifelong Learning" of the National Strategic Reference Framework (NSRF) - Research Funding Program: "Thales – Democritus University of Thrace – Center for Multifunctional Nanocomposite Construction Materials" (MIS 379496). The second author also acknowledges the support of the University of Cyprus.

## Notation

$E$  = Modulus of Elasticity

$F$  = interparticle forces

$G_f$  = fracture energy

$U$  = lattice energy of the composite

$U_f$  = lattice energy associated with the fiber net

$U_h$  = lattice energy of the hydrate

$V_f$  = volumetric ratio of fibers in the hydrate

$M_f$  = weight ratio of fibers per weight of cement

$c$  = weight of cement per unit volume of hydrate

$g_c$  = density of cement

$g_f$  = density of fibers

$f_{CN}^{max}$  = nominal development capacity of a CNT in the binder

$f_{CN}$  = axial stress in CNT

$\overline{f}_{CN}$  = mean value of  $f_{CN}$

$f_t, f_{t,CNT}$  = tensile strength of the material without and with CNT reinforcement

$n_{CN}$  = number of strings crossing a unit area of the composite

$n_C$  = principal compressive stress in the composite

$n_T$  = principal tensile stress in the composite

$r_o$  = hydraulic mean radius

$w$  = crack mouth opening displacement (cmo)

$\varepsilon_f$  = average tensile strain in the composite – taken equal with mean fiber strain in the direction of the load

$\theta_f$  = angle of fiber orientation relative to a reference plane

$\lambda_{eff}$  = fiber effectiveness coefficient

$k_{CN}$  = average isotropic stiffness of the CNT/CNF system in the binder mass

$\alpha_{CN}$  = area of a single CNT

$\delta$  = separation distance

$\delta_o$  = equilibrium separation distance

## References

Abu Al-Rub R., Ashour A. and Tyson B. (2012a), "On the aspect ratio effect of multi-walled carbon nanotube reinforcements on the mechanical properties of cementitious nanocomposites", *Constr. Build.*

- Mater.*, **35**, 647-655.
- Abu Al-Rub, R., Tyson, B., Yazdanbakhsh, A. and Grasley, Z. (2012b), "Mechanical Properties of nanocomposite cement incorporating surface-treated and untreated carbon nanotubes and carbon nanofibers", *ASCE J. Nanomech. Micromech.*, **2**, 1-6.
- Balaguru, P.N. and Shah, S.P. (1992), *Fiber reinforced Cement Composites*, McGraw-Hill Inc., N.Y.
- Bharj, Jyoti, Sarabjit Singh, Subhash Chander and Rabinder Singh, (2014), "Experimental study on compressive strength of cement-CNT composite paste", *Indian J. Pure Appl. Phy.*, **52**, 35-38
- Chaipanich, A., Nochaiya, T., Wongkeo, W. and Torkittikul, P. (2010), "Compressive strength of microstructure of carbon nanotubes-fly ash cement composites", *Mater. Sci. Eng., A* **527**, 1063-1067.
- Cwirzen, A., Habermehl-Cwirzen, K. and Penttala, V. (2008), "Surface decoration of carbon nanotubes and mechanical properties of cement/carbon nanotube composites", *Adv. Cement Res.*, **20**(2), 65-73
- Dwivedi, N., Kumar, S., Malik, H.K., Govind, Rauthan, C.M.S. and Ranwar, O.S. (2011), "Correlation of sp<sup>3</sup> and sp<sup>2</sup> fraction of carbon with electrical, optical and nano-mechanical properties of argon-diluted diamond-like carbon films", *Appl. Surf. Sci.*, **257**, 6804-6810.
- Ferro G., Tulliani J.M. and Musso, S. (2011) "Carbon nanotubes cement composites", *Proceedings, Frattura ed Integrita Strutturale*, **18**, 34-44, DOI 10.3221/IGF-ESIS.18.04
- Fib Model Code (2010), Federation International du Beton, Lausanne, <http://www.fib-international.org/model-code-2010-first-complete-draft-vol-1>.
- Hlavacek, P., Smilauer, V., Padevet, P., Nasibulina, L. and Nasibulin, A. (2011), "Cement grains with surface synthesized carbon nanofibres: Mechanical properties and nanostructure", *CD-ROM Proceedings, Nanocon, 9/2011*, Brno, Check Republic.
- Konsta-Gdoutos, M.S., Metaxa, Z.S. and Shah S.P. (2010), "Carbon nanofiber-reinforced cement-based materials", *J. Transport. Res. Board*, No. 2142, Washington, D.C., 114-118.
- Konsta-Gdoutos, M.S., Metaxa, Z.S. and Shah, S.P. (2010), "Highly dispersed CNTs reinforced cement-based materials", *Cement Concrete Res.*, **40**(7), 1052-1059.
- Konsta-Gdoutos, M.S., Metaxa, Z.S. and Shah, S.P. (2010), "Multi-scale mechanical and fracture characteristics and early-age strain capacity of high performance carbon nanotube/cement nanocomposites", *Cement Concrete Compos.*, **32**(2), 110-115.
- Kumar, S., Kolay P., Mala, S. and Mishra, S. (2012) "Effect of multiwalled carbon nanotubes on mechanical strength of cement pastes", *ASCE J. Mater. Civil Eng.*, **24**(1), 84-91.
- Li G.Y., Wang P.M. and Zhao X., (2005) "Mechanical behavior and microstructure of cement composites incorporating surface-treated MWCNTs", *Carbon*, **43**, 1239-1245.
- Li V.C. (2003), "On Engineered cementitious composites (ECC)", *J. Adv. Concrete Technol.*, **1**(3), 215-230.
- Makar, J.M. and Beaudin, J.J. (2004), "Carbon nanotubes and their applications in the construction industry," in "Nanotechnology in construction", *1st Intl. Symp. Nanotechnology in Construction*, 331-341.
- Metaxa, Z.S., Konsta-Gdoutos, M.S. and Shah, S.P. (2009), "Carbon nanotubes reinforced concrete", *ACI SP 276-2*, 11-19.
- Metaxa, Z.S., Konsta-Gdoutos, M.S. and Shah, S.P. (2011), "Mechanical properties and nanostructure of cement-based materials reinforced with carbon nanofibers and polyvinyl alcohol (PVA) microfibers", *ACI SP, 270-10*, 115-124.
- Morsy, M.S., Alsayed, S.H. and Aqel, M. (2011), "Hybrid effect of CNT and nano-clay on physic mechanical properties of cement mortar", *Constr. Build. Mater.*, **25**, 145-149.
- Musso, S., Tulliani, J.M., Ferro, G. and Tagliaferro, A. (2009), "Influence of carbon nanotubes structure of the mechanical behavior of cement composites", *Compos. Sci. Technol.*, **69**, 1985-1990.
- Peled, A., Cyr, M. and Shah, S.P. (2000), "Hybrid fibers in high performances extruded cement composites", *5th Intern. RILEM Symp.*, BEFIB, Lyon, France.
- Pantazopoulou S.J. and Mills R.H. (1995), "Microstructural aspects of the mechanical response of plain concrete", *ACI Mater. J.*, **92**(6), 605-616, November-December.
- Pantazopoulou, S.J. and Zanganeh, M. (2001), "Triaxial tests of fiber reinforced concrete", *ASCE J. Mater.*

- Civil Eng.*, **13**(5), 340-348.
- Sakulich, A.R. and Li, V.C. (2011), “Nanoscale characterization of engineered cementitious composites (ECC)”, *Cement Concrete Res.*, **41**, 169–175.
- Shah, S.P., Konsta-Gdoutos, M.S., Metaxa, Z.S. and Mondal, P. (2009), “Nanoscale modification of cementitious materials”, *Nanotech. Constr.* 3, (Eds.: Z. Bittnar, P.J.M. Bartos, J. Nemecek, V. Smilauer, J. Zeman, Springer, pp. 125-130.
- Shi, C.J. and Mo, Y.L. (2008), “High-performance construction materials: Science and applications, Vol. 1, Engineering materials for technological needs”, World Scientific, ISBN 981279736X, 9789812797360, 431pp.
- Sobolkina, A., Mechtcherine, V., Khavrus, V., Maier, D., Mende, M., Ritchel, M. and Leonhardt, A. (2012), “Dispersion of Carbon Nanotubes and its influence of the mechanical properties of the cement matrix”, *Cement Concrete Compos.*, **34**, 1104-1113.
- Tastani, S.P. and Pantazopoulou, S.J. (2006), “Bond of G-FRP bars in concrete: Exper. study and analytical interpretation”, *ASCE J. Compos. Constr.*, **10**(5), 381-391.
- Tyson, B., Abu Al-Rub, R., Yazdanbakhsh, A. and Grasley, Z. (2011), “Carbon nanotubes and carbon nanofibers for enhancing the mechanical properties of nanocomposite cementitious materials”, *ASCE Mater. J. Civil Eng.*, **23**(7), 1027-1035.
- Wang, C., Li, K.Z., Li, H.J., Jiao, G.S., Lu, J.H. and Hou, D.S. (2008), “Effect of carbon fiber dispersion of the mechanical properties of the carbon FRC composites”, *Mater. Sci. Eng.*, **A:487**, 52-57.